

Thermal, optical, electrical and structural study of new symmetrical azomethine based on poly(1,4-butanediol)bis(4-aminobenzoate)

Agnieszka Iwan^{a,*}, Pawel Bilski^b, Henryk Janeczek^c, Bozena Jarzabek^c, Marian Domanski^c, Patrice Rannou^d, Andrzej Sikora^a, Damian Pociecha^e, Bozena Kaczmarczyk^c

^aElectrotechnical Institute, Division of Electrotechnology and Materials Science, M. Skłodowskiej-Curie 55/61 Street, 50-369 Wrocław, Poland

^bInstitute of Nuclear Physics, Polish Academy of Sciences, Radzikowskiego 152 Street, 31-342 Krakow, Poland

^cCentre of Polymer and Carbon Materials, Polish Academy of Sciences, 34 M. Curie-Skłodowska Street, 41-819 Zabrze, Poland

^dLaboratoire d'Electronique Moléculaire, Organique et Hybride, UMR5819-SPRAM (CEA-CNRS-Univ. J. FOURIER-Grenoble 1), INAC Institut Nanosciences & Cryogénie, CEA-Grenoble, 17 Rue des Martyrs, 38054 Grenoble Cedex 9, France

^eUniversity of Warsaw, Department of Chemistry, Zwirki i Wigury 101, 02-089 Warsaw, Poland

ARTICLE INFO

Article history:

Received 20 August 2009

Received in revised form 20 October 2009

Accepted 20 October 2009

Available online 23 October 2009

Keywords:

Azomethines

Imines

Liquid crystals

Photoluminescence

Thermoluminescence

Current–voltage measurements

ABSTRACT

The synthesis, characterization and mesomorphism of new thermotropic imine prepared via condensation of biphenyl-4-carboxaldehyde with poly(1,4-butanediol)bis(4-aminobenzoate) was reported. The structure of imine was characterized by means FTIR, ¹H, ¹³C NMR spectroscopy and elemental analysis; the results show an agreement with the proposed structure. The differential scanning calorimetry, polarizing optical microscopy and X-ray diffraction (WAXRD, SAXRD) were employed to evaluate their phase transitional behavior. The imine exhibited smectic A (SmA) and smectic B (SmB) mesophases. Liquid crystalline properties of the azomethine were studied additionally via UV–vis spectroscopy in the function of temperature (UV–vis(T)). The compound has one emission band at 360 nm and thermoluminescence emission occurs at about 500–600 nm wavelengths. Current–voltage measurements were performed on ITO/AZ/Alq₃/Al device with three different thickness of the film.

© 2009 Elsevier B.V. All rights reserved.

1. Introduction

The development of new materials based on self-organizing systems has had a great deal of attention due to their potential in the construction of well-defined supramolecular nanostructures. Self-assembling molecules, which include liquid crystals (LC), block copolymers, hydrogen bonded complexes and coordination polymers are widely studied for their great potential as advanced functional materials [1–8]. Liquid crystals, made up of rod-like molecules, exhibit novel supramolecular architecture and have found novel use in optoelectronic applications i.e., flat panel displays (FPDs). The azomethines called also Schiff bases or imines are widely investigated as liquid crystalline materials. LC, rod shaped, symmetrical azomethines, being also under consideration in the present paper, have been examined in the following papers [9–21].

Azomethines i.e., compounds containing CH=N– groups in the main chain, being isoelectronic with the corresponding *p*-phenylene vinylene, exhibit interesting electronic, luminescent and non-linear optical properties [8,12,20]. The principal feature of the azomethines which distinguishes them from the majority of

conjugated compounds is the presence of basic centres associated with imine nitrogen. This implies that acid–base chemistry can be used for the modification of the compound properties.

Inspired by the above described findings we have undertaken a detailed study of the structure–spectroscopic–thermal properties in a new azomethine (abbreviated hereinafter as AZ). In this work we will present the thermal (POM, DSC), optical (UV–vis, photo- and thermoluminescence), electrical (current–voltage) measurements and structural (AFM, X-ray) characterizations of calamitic azomethine. The LC behavior as well as photo- and thermoluminescence properties of the symmetrical azomethine based on the structure poly(1,4-butanediol)bis(4-aminobenzoate) were not investigated so far.

In this paper, we will present full characterization of the LC azomethine of great interest for the emerging field of (supra)molecular electronics and for their uses as active layers in optoelectronic devices (LEDs, FETs, Solar Cells, Lasers).

2. Experimental section

2.1. Synthesis

All chemicals and reagents were used as received from Aldrich.

* Corresponding author.

E-mail address: a.iwan@iel.wroc.pl (A. Iwan).

2.1.1. Synthesis of 4,4'-(butane-1,4-diylbis(oxy)bis(butane-4,1-diyl)-bis(4-(biphenyl-4-ylmethyleneamino)benzoate) (AZ)

Poly(1,4-butanediol)bis(4-aminobenzoate) (PBBA, mp. 56 °C) (1 mmol) and biphenyl-4-carboxaldehyde (mp. 57–59 °C) (2 mmol) were added in a glass reactor fitted with stirrer. The reaction mixture was purged with nitrogen for 30 min, and then the temperature was raised to 170 °C and kept on for 24 h under positive pressure of nitrogen. The mixture was then cooled to room temperature, scraped and powdered. The crude product was washed three times with methanol (3 × 500 ml) and next two times with acetone (2 × 350 ml) to remove unreacted compounds. Finally the azomethine was dried at 60 °C under vacuum for 24 h to give the AZ (88%).

¹H NMR (300 MHz, CDCl₃, TMS) [ppm] δ 8.47 (s, 2H, 2 × CH=N); 8.07–8.10 (d, 4H, orto position to –O–C=O); 7.97–7.99 (d, 4H, 4 × H_{Ar}); 7.64–7.74 (m, 8H, 8 × H_{Ar}); 7.45–7.50 (m, 2H, 2 × H_{Ar}); 7.30–7.39 (m, 4H, 4 × H_{Ar}); 7.24–7.26 (m, 4H, 4 × H_{Ar}, orto position to N=CH); 4.36 (m, 4H, 2 × CH₂–O–CO); 3.46–3.51 (m, 8H, 4 × CH₂–O); 1.64–1.87 (m, 12H, (CH₂)₆).

¹³C NMR (75 MHz, CDCl₃, TMS) [ppm] δ 166.37 (–O–CO); 161.19 (CH=N); 156.19 (–C_{Ar}–N=); 140.09 (C_{Ar}–C_{Ar}–); 131.55 (C_{Ar}–CH=N–); 130.84; 130.27 (C_{Ar}–, orto position to O–CO–); 129.53; 129.00; 128.92; 128.46; 128.02; 127.68; 127.62; 127.50; 127.35; 127.18 (C_{Ar}– in Ph–Ph); 120.69 (C_{Ar}– at orto position to –N=CH); 70.72; 70.35; 70.24 (–CH₂–O–); 64.79; 64.16 (–CH₂–O–CO–); 26.49; 26.39; 25.66 (–CH₂–CH₂–).

FTIR (KBr)/cm⁻¹: 3055 (ν CH_r), 3035 (ν CH_r), 2939 (ν_{as} CH₂), 2862 (ν_s CH₂), 2804 (ν_s CH₂), 1712 (ν C=O), 1625 (ν C=N), 1595 (ν Ph), 1561 (ν Ph), 1520 (ν Ph), 1487 (δ CH₂), 1471 (δ CH₂), 1450 (ν Ph), 1411 (ν Ph), 1372 (δ CH₂), 1364 (δ CH₂), 1339 (ω CH₂), 1306 (ω =CH_r), 1287 (τ CH₂), 1253 (ν (C=O)–O), 1191 (ν Ph–N=), 1169 (δ CH_r), 1123 (δ CH/νCOC), 1114 (δ CH/νCOC), 1100 (δ CH_r), 1047 (δ CH), 1007 (δ CH_r/ν CO), 987 (γ CH_r), 972 (γ CH_r), 891 (γ CH_r/νCOC), 853 (ρ CH₂), 834 (γ CH_r), 771 (γ CH_r), 759 (ν Ph), 732 (γ CH_r/skel. CH₂), 719 (γ Ph), 698 (γ Ph), 688 (γ Ph), 668 (δ Ph) where: ν – stretching vibrations, δ – in-plane deformation, γ – out-of-plane deformation, Ph – phenyl, ν – stretching vibrations, δ – in-plane deformation, γ – out-of-plane deformation, ω – wagging, ρ – rocking, τ – twisting, skel. – skeletal vibrations, Ph – phenyl, CH_r – CH group in phenyl ring.

Tg, 23.8 °C (10 deg/min); Anal. Calcd. for C₅₂H₅₂N₂O₆ (800.979): C, 77.97%; H, 6.54%; N, 3.50%. Found: C, 77.64%; H, 6.46%; N, 3.75%.

2.2. Instruments

Synthesized compound was characterized by ¹H NMR and elemental analysis. Compound was also characterized by Fourier transform infrared (FTIR) and ultraviolet–visible (UV–vis) absorption spectroscopy. NMR was recorded on a Bruker AC 200 MHz. Chloroform-*d* (CDCl₃) containing TMS as an internal standard was used as solvent. Elemental analyze (C, H and N) was recorded on a 240C Perkin-Elmer analyzer. Infrared spectrum (FTIR) was acquired on a DIGILAB FTS-40A Fourier transform infrared spectrometer in the range of 4000–400 cm⁻¹ at a resolution of 2 cm⁻¹ and for an accumulated 32 scans. Sample was analyzed as pellets in potassium bromide.

Solution (THF) UV–vis absorption spectra were recorded *in situ* during analytical size-exclusion chromatography (SEC) analyses using the diode array detector (DAD) of a Hewlett-Packard 1100 Chemstation equipped with a 300 × 7.5 mm Polymer labs PLgel Mixed-D 5 μm/10⁴ Å column, a DAD detector and a refractive index (RI) detector.

Solution photoluminescence (PL) spectra were recorded at RT on a Hitachi F-4500 spectrometer using diluted THF solution showing an absorption level of. ca. 0.1 absorbance unit at the wavelength chosen for their excitation.

Current–voltage characteristics were detected using electrometer Keithley 6715. Current–voltage measurements were performed on ITO/AZ/Alq₃/Al device. Alq₃ layer was vacuum deposited on top of the ITO/AZ layer at a base pressure of ca. 10⁻⁶ Torr and then Al electrode was vacuum deposited at the same pressure. The area of the diodes was 9 mm².

The surface morphology investigation of the AZ was performed in air using a commercial Innova company Veeco Co. Atomic Force Microscopy (AFM) in the contact and uncontact mode. Measurements were done in Tapping Mode and Phase Imaging. Also Local Contrast was made.

The phase transitions and mesogenicity were studied by differential scanning calorimetry (DSC) and polarizing microscope observations (POM). DSC were measured on a TA-DSC 2010 apparatus using sealed aluminium pans under nitrogen atmosphere.

The textures of their mesophases were observed with a POM setup composed of: (i) a LEICA DMLM Microscope working in both transmission and reflexion modes and equipped with a set of lenses allowing magnification by 2.5×, 5×, 10×, 20× and 50×, (ii) a LINKAM LTS350 (–196 °C till +350 °C) hot plate and a LINKAM CI94 temperature controller, (iii) a JVC Numeric 3-CCD KYF75 camera (resolution: 1360 × 1024).

Small angle X-ray diffraction (SAXRD) experiments were performed with Bruker NanoStar setup (Cu Kα radiation, crossed-coupled Goebel mirrors, Vantec 2000 area detector). Temperature of the sample, placed in thin walled glass capillary (1 mm), was controlled using MRI TCPU H heating stage. Wide angle X-ray diffraction (WAXRD) was conducted on Bruker D8 GADDS system (Cu Kα radiation, Goebel mirror, Hi-Star area detector). Sample was prepared as a droplet on a heated surface.

UV–vis spectra in different temperatures were measured for thin film on the quartz (film cast from dichloroethane) by JASCO V-570 UV–vis-NIR spectrometer using a temperature-controlled optical cell in a temperature range from the room temperature to clearing point in the heating process.

Thermoluminescent (TL) measurement was realized using the RA'94 TL Reader/Analyzer. It is equipped with a platinum planchet heater and a photomultiplier with a bialkali photocathode. The AZ sample was irradiated with a test dose of 23 Gy Cs-137 gamma-rays. Measurements were performed with a linear heating ramp at a rate of 1 K/s up to temperature of 420 K. At this temperature sample was totally liquidized.

3. Results and discussion

3.1. Synthesis and characterization

In general, the condensation of amines with aldehydes efficiently takes place in different solvents in the presence of the catalyst. The condensation of poly(1,4-butanediol)bis(4-aminobenzoate) (PBBA) with biphenyl-4-carboxaldehyde, did not proceed in these reaction conditions (see Table 1). In our opinion it is caused by low reactivity of the PBBA.

It is well known that the azomethine carbon has poor electrophilicity and has the tendency of enolizable imines and imine derivatives [22]. Additionally, there are many factors that can be altered in order to drive the reaction forward such as solvent, concentration, pH and temperature. For an imine bond formation (it means dynamic reaction) the change in the free energy during the reaction must be favourable, i.e., ΔG° in equation ΔG° = ΔH° – TΔS° must be less than zero. Moreover, many external considerations, including steric and electronic factors can influence on the progress of the reaction.

Azomethine described in this paper was prepared via high temperature melt condensation at 170 °C. Substrates were introduced

Table 1
Optimization of the reaction conditions of the azomethine.

Solvent	Catalyst	Temperature (°C)	Time (h)	Yield (%)
Chloroform	PTS, LiCl, DABCO, DMAP, DABCO/TiCl ₄	b.p.	12, 24, 48	0
DMA	PTS, LiCl, DABCO, DMAP, DABCO/TiCl ₄	100, 120, 150, 170	12, 24, 48	0
NMP	PTS, LiCl, DABCO, DMAP, DABCO/TiCl ₄	100, 120, 150, 170	12, 24, 48	0
<i>m</i> -krezol	PTS, LiCl, DABCO, DMAP, DABCO/TiCl ₄	100, 120, 150, 170	10, 24, 48	0
–	–	170	24	88

b.p., boiling point of the solvent; PTS, *p*-toluenesulfonic acid; DABCO, 1,4-diazobicyclo[2,2,2]octane; DMAP, 4-dimethylamino-pyridin; DMA, *N,N*-dimethylacetamide; NMP, 1-methyl-2-pyrrolidinone.

into a 20-ml, two-necked, round-bottomed flask equipped with an overhead stirrer and a nitrogen inlet. The crude product was washed three times with methanol and next two times with acetone to remove unreacted diamine and aldehyde. Additionally, the compound was characterized by thin layer chromatography (TLC) (developing solvent dichloroethane/ethyl acetate, 50/50). Analytical thin layer chromatography (TLC) was performed on silica gel plates from E. Merck (silica gel F₂₅₄). Additionally, the mass dispersion of the AZ was examined by SEC method (polystyrene standards were used). A single narrow SEC band found for the AZ clearly indicated a monodisperse distribution of the imine molecular masses and thereby additionally proved height purity of the compound synthesized. Azomethine yield was 88%. The compound was soluble at room temperature in chloroform, THF, DMA and DMF. The azomethine was characterized by FTIR, NMR spectroscopy and elemental analysis. The synthetic pathway along with chemical structure of the azomethine synthesized in this research is presented in Fig. 1 whereas their principal spectroscopic and molecular characteristics are collected in Experimental section. The spectral data were in accordance with the expected formula.

The absence of the residual amino (NH₂) and aldehyde (CHO) groups together with the appearance of band typical for azomethine bonds (HC=N–) was confirmed by FTIR and NMR spectra. The spectra have assessed their purity and confirmed their molecular structure. In particular the signal about 161 ppm, present in the ¹³C NMR spectrum of the compound, confirms the existence of the azomethine group carbon atoms. In proton NMR spectrum of the investigated compound the imine proton signal at 8.47 ppm was observed. Additionally, in FTIR spectrum the imine vibration at about 1625 cm⁻¹ was observed.

3.2. Optical properties

The photophysical properties of AZ were investigated using UV–vis and photoluminescence spectroscopy. The UV–vis absorbance spectrum of the AZ in THF solution displayed one absorption maximum at 296 nm and hump at 350 nm. The fluorescence (emission)

spectrum in THF solution (1.25 × 10⁻³ M) at room temperature was recorded for the 296 and 325 nm excitation wavelength. Independently on the excitation wavelength the azomethine AZ exhibited one emission band at 360 nm (Fig. 2). The Stokes shift for the AZ was 66 nm. These spectroscopic data ascertained the fluorescence properties of this symmetrical azomethine.

3.3. Current–voltage characteristics

Current–voltage measurements were performed on ITO/AZ/Alq₃/Al device. The azomethine solution (1 w/v% in dichloroeth-

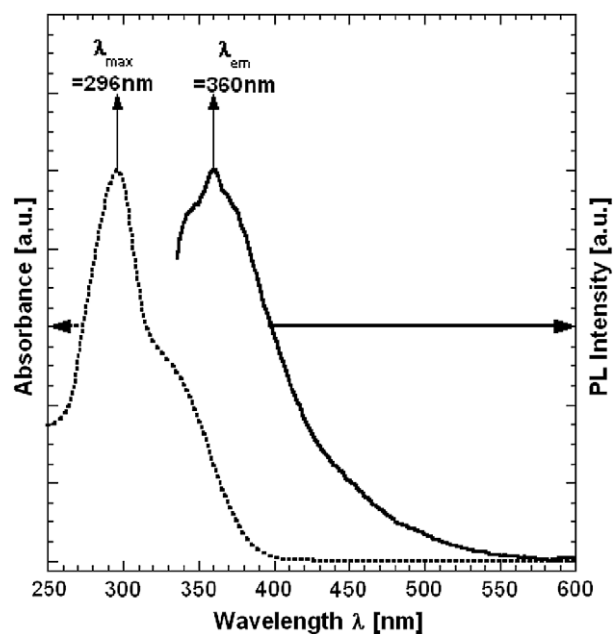


Fig. 2. Absorption (UV–vis) and emission (photoluminescence) spectra of the AZ in THF solution.

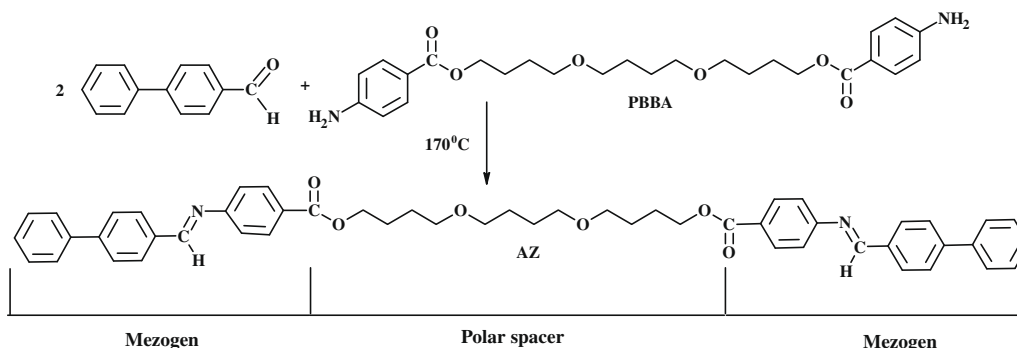


Fig. 1. Synthetic route and chemical structure of the azomethine.

ane) was spin-cast onto ITO-covered glass substrate at room temperature in order to produce a thin hole transporting layer (HTL). Residual traces of solvent were removed by heating the film in a vacuum. The green emitting Alq₃ layer was vacuum deposited on top of the HTL layer at a base pressure of ca. 10⁻⁶ Torr and then Al electrode was vacuum deposited at the same pressure. The area of the diodes was 9 mm². Current–voltage (I–V) curves of ITO/AZ/Alq₃/Al devices investigated in room temperature are shown in Fig. 3. Differences were found along with change the thickness of the film from 150 to 250 nm. It can be seen that for the thickness of the film about 150 nm current rapidly increases with applied voltage increase. The turn-on voltage of this device was observed at about 2 V in room temperature.

On the other hand the turn-on voltage of the devices with thickness of the film about 200–250 nm was similar and was observed at

about 12 V in room temperature. Additionally, for these devices we did not observed quick current increases along with applied voltage increase. This behavior confirmed the influence of the thickness of the layer on the electrical properties of the compound. The differences found in the I–V characteristic of the imine confirm the difference planarity of the imine structure and different conformations of the compound in film with various thicknesses.

3.4. AFM analysis

AZ film on the typical microscopic glass substrate was obtained by dissolving at room temperature the compounds in chloroform to form a homogenous solution. Residual solvent was removed by heating the film. Film of the AZ obtained by casting from chloroform solution shows a very interesting morphology, characteristic of systems capable of forming organized supramolecular structures. The surface morphology investigation of the AZ was performed in air using an Atomic Force Microscope (AFM) in the intermittent contact mode. The *Inclination* transformation of the topography was made in order to provide better view of the structures. Additionally, the surface potential imaging (SP) was performed in order to obtain information about homogeneity of electrical properties of the surface. Obtained images of the AZ in different range of scan (1000 and 500 nm, respectively) are presented in Fig. 4 in order they were mentioned above.

The film of the AZ obtained by casting from chloroform solution on glass substrate showed ordered, planar-oriented morphology (see Fig. 4). AFM images of the AZ, revealed terraces-like organizational features as we could clear seen in the *Inclination* transformation. One can note the “steps” of few nanometers (5–12 nm) in height, creating main relief of the topography. After careful study of the picture (4b), one can see also a number of edges of very small terraces covering all surface of the sample. The height of single layer is about 0.15 nm. It reveals layered structure of the sample.

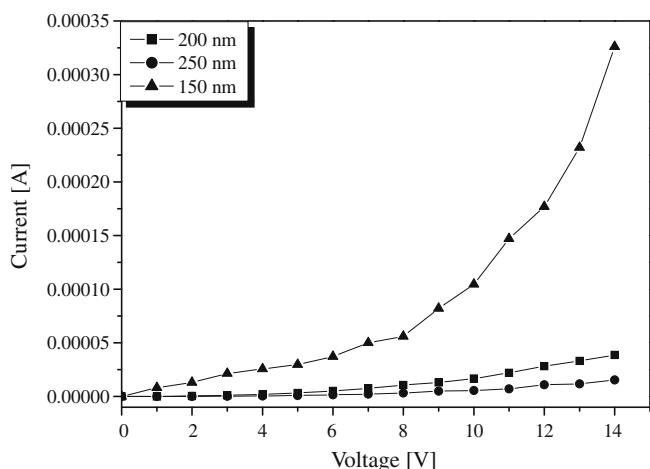


Fig. 3. Current–voltage curves of device ITO/azomethine/Alq₃/Al (thickness about 150, 200 and 250 nm).

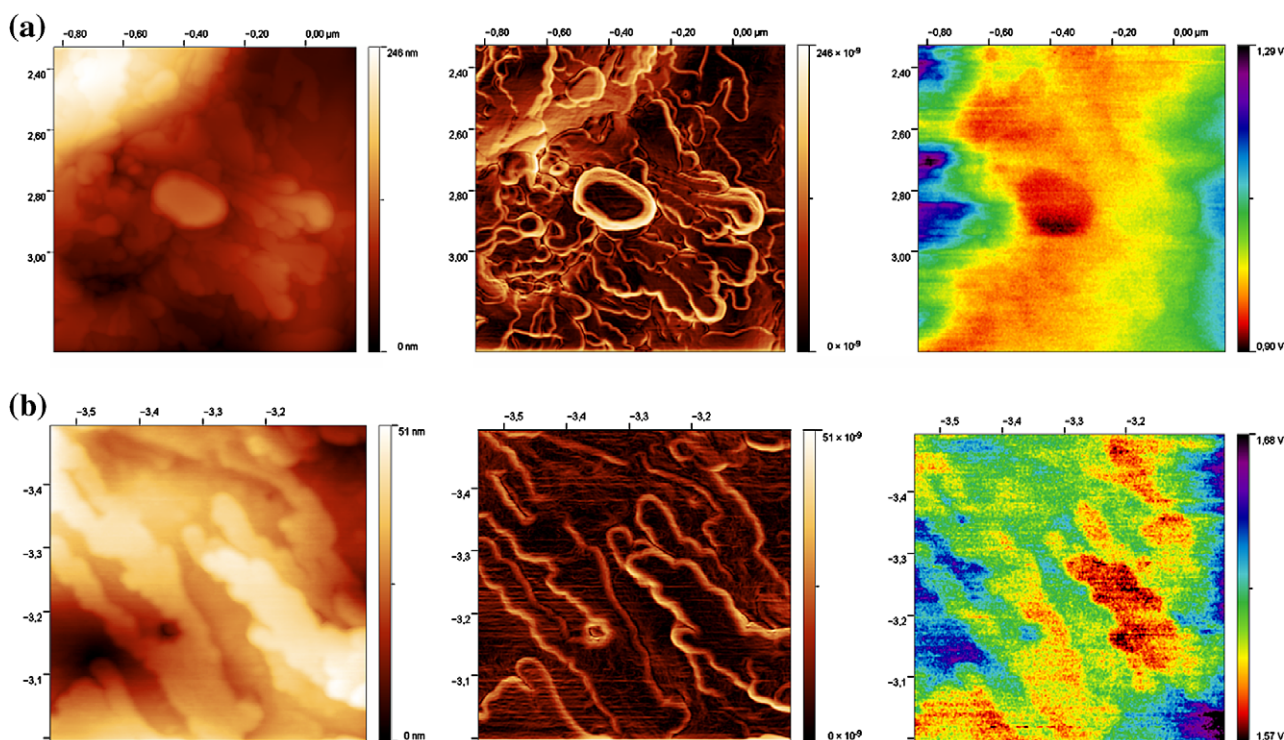


Fig. 4. AFM images of the AZ coated from chloroform solution. Left side: AFM topography images, middle transformation *Inclination*, right side: surface potential (a) surface pattern 20×20 μm², Rms: 50 nm, (b) surface pattern 0.5×0.5 μm², Rms: 9.95 nm.

The slopes of large terraces are as a matter of fact made of a large group of elementary layers placed very close to each other.

3.5. Liquid crystalline properties

Liquid crystal properties of the AZ were investigated mainly with the help of differential scanning calorimetry (DSC), polarizing optical microscope (POM) and X-ray diffraction. The tentative mesophases identifications and the sequence of phase transitions related to the AZ are based on the identification of textures appearing in two reference textbooks for liquid crystals [23,24] and on repeated POM and DSC experiments. Liquid crystalline properties of the azomethine AZ were additionally studied by UV–vis spectroscopy in different temperatures (UV–vis(T)) and thermoluminescence (TL).

3.5.1. DSC and POM study

Upon DSC analysis the AZ exhibited two enantiotropic transitions such as crystal-to-mesophase (Cr/M) and mesophase-to-isotropic state (M/I). DSC curves of the AZ during second cooling and heating scan (1 deg/min), along with the DSC curves of the AZ during first heating scan (10 deg/min) and heating scan after quenching (15 deg/min) are presented in Fig. 5a and b and 5c, respectively. Compound AZ showed a liquid crystal to isotropic transition at 149.8 °C with a $\Delta H = 8.7$ J/g on the heating rate 1 deg/min (Fig. 5a). On cooling from the isotropic state to room temperature, an exothermic peak appeared at 147.2 °C with a $\Delta H = 8.9$ J/g, corresponding to the transition from the isotropic state to the liquid crystalline phase (Fig. 5a). Moreover, it should be noted that during heating of the sample (after rapid cooling) so called “cold” crystallization was found at 88.9 °C (Fig. 5a). This behavior was not observed for the AZ during first heating scan (Fig. 5b). Details of the transition temperatures and associated enthalpy change of the AZ, as determined by DSC are summarized in Table 2.

The POM measurements revealed textures which could indicate SmA and SmB mesophases. Details of transition temperatures of the compound AZ as determined by POM are summarized in Table 2 together with their phase variants.

The microphotographs of the smectic phases obtained for the compound AZ are shown in Fig. 6.

The SmA mesophase of the AZ showed a focal conic fan texture (Fig. 6). We did not manage to catch a POM image (observed during a cooling scan) at the SmA > SmB transition with the typical so-called transition bars. Nevertheless we are quite confident that SmB > SmA transition and SmA > SmB occurred at 125 °C and at 120 °C during heating and cooling scans, respectively. These observations were confirmed by DSC study of the sample during the first heating scan at 10 deg/min and heating rate 15 deg/min after quenching (Table 2). On DSC thermogram presented in Fig. 5b two endotherms at 124.6 °C and at 154.9 °C before isotropisation were found during heating of the sample at 10 deg/min. Similar behavior was observed during heating of the sample at 15 deg/min after quenching (see Table 2 and Fig. 5c). These observations are in quite good agreement with DSC measurement of the sample during cooling of the sample at 1 deg/min (Fig. 5a). After a first exotherm with a maximum at 147.2 °C another exotherm is sluggishly developing from ca. 115 °C to its maximum at ca. 99.2 °C. We suppose that this last exotherm is in fact consisting of 2 consecutive exotherms characteristics of a SmA > SmB transition followed by a SmB > Frozen SmB and/or Cr transition.

The paramorphotic (i.e., because its look is depending on the existence of a previous focal conic fan texture of a SmA mesophase) focal conic fan texture of the SmB mesophase (see Fig. 6) of AZ is quite difficult to differentiate with the one of its SmA mesophase as no typical transitory transition bars appeared during cooling

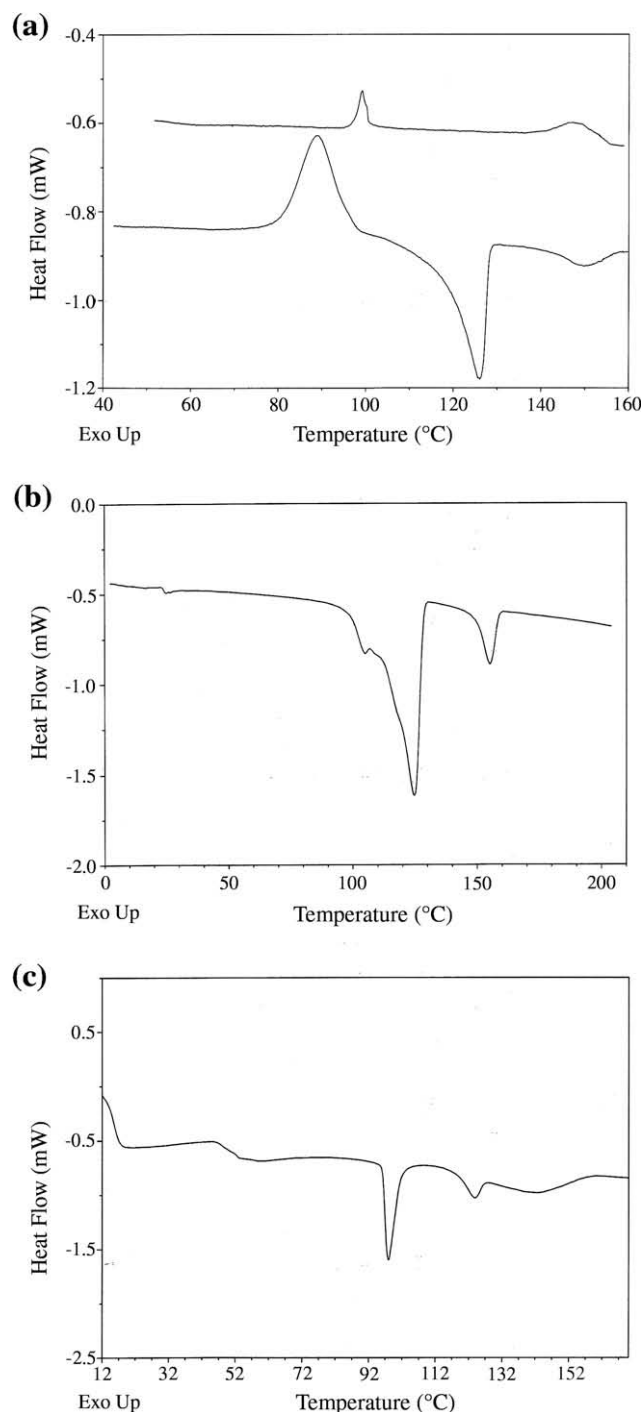


Fig. 5. DSC curves of the AZ obtained on (a) the heating and the cooling rate 1 deg/min under N₂ atmosphere. The temperature range from 40 to 160 °C, (b) the heating rate 10 deg/min under N₂ atmosphere. The temperature range from 0 to 200 °C and (c) the heating rate 15 deg/min after quenching under N₂ atmosphere. The temperature range from 12 to 160 °C.

or heating scans. However, at the bottom left corner of POM images more white parts were observed for the focal conic fans in Fig. 6b than in Fig. 6a.

While a SmA mesophase shows a 1D (lamellar) organization (with no positional order within a layer), going to a more ordered orthogonal smectic phase could lead to two closely related SmB mesophases which show the same POM textures and that can only be distinguished by X-ray: the so-called hexatic smectic B mesophase (SmB_{Hex}: an orientational order of local crystallographic

Table 2

Phase transition temperature (°C) of the compound detected by POM and DSC along with enthalpy values, ΔH (J/g).

Phase transitions, cooling, POM	
Cr (or frozen SmB)	97.5, SmB 120, Sm A 156.5, I
Phase transitions, heating, POM	
Cr (or frozen SmB)	105, SmB 125.5, Sm A 158.5, I
Phase transitions, cooling, DSC, [ΔH]	
Cr (or frozen SmB)	99.2 [5.5], SmB 115, Sm A 147.2 [8.9], I
Phase transitions, heating, DSC, [ΔH] [*]	
"cold" Cr	88.9 [51.8], SmB 126.1 [56.5], Sm A 149.8 [8.7], I
Phase transitions, heating, DSC, [ΔH] ^{**}	
mp.	104.4, SmB 124.6, SmA 154.9 [11.0], I
Phase transitions, heating, DSC, [ΔH] ^{***}	
"cold" Cr	89.2 [19.3], SmB 125.9, SmA 146.4 [6.6], I
Phase transitions, heating, DSC, [ΔH] ^{****}	
"cold" Cr	45.3 [3.4], mp. 97.9 [5.0], SmB 123.7 [1.3], SmA 142.6 [2.9], I

Cr, SmA, SmB, and I indicate crystal, smectic A, smectic B, and isotropic phases, respectively.

* Cooling 1 deg/min.

** Heating 1 deg/min.

*** Heating 10 deg/min.

**** Heating 10 deg/min after slow cooling.

***** Heating 15 deg/min after quenching, mp, melting point.

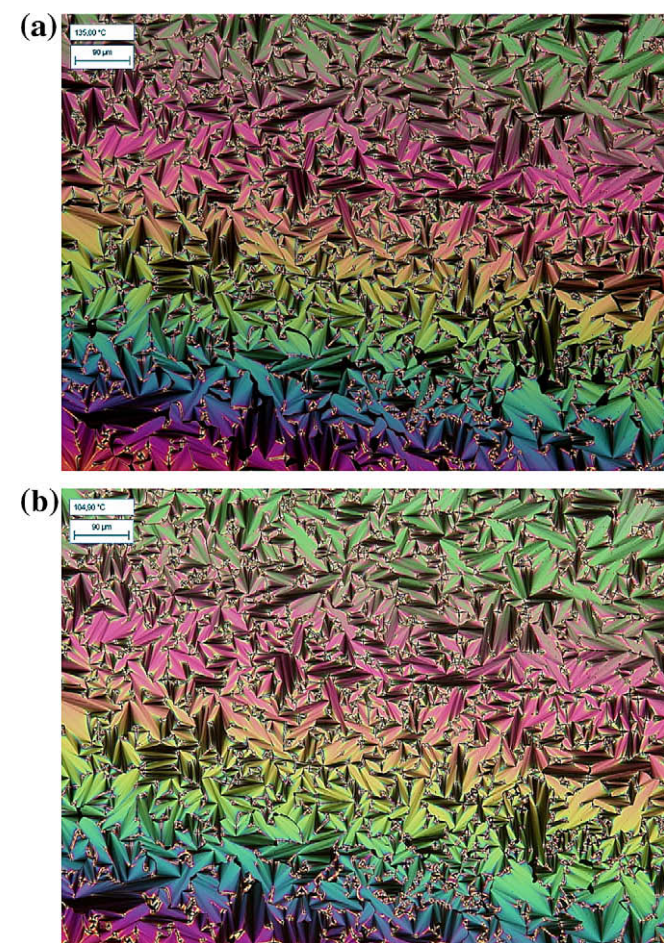


Fig. 6. Photomicrographs of the optical textures of mesophases obtained for the AZ (a) SmA, focal conic (seen at 135 °C) and (b) SmB, paramorphic focal conic (seen at 104.9 °C).

axes, called Bond Orientational Order, develops within the layer, without long-range positional order) and the so-called crystal B mesophase ($\text{SmB}_{\text{Cryst}}$: a hexagonal lattice develops within the layer

with long-range positional correlations of molecular mass centres). In the above-mentioned proposed scenario of phase transitions, we just indicated that the second mesophase observed on cooling from the isotropisation state is a SmB.

3.5.2. X-ray(T) study

X-ray diffraction revealed lamellar structure of mesophases of studied compound, in agreement with proposed designation of SmA and SmB phases. Layer spacing in smectic phases, $d \sim 27$ Å, only weakly depends on temperature, interestingly there is no pronounced increase of layer thickness on transition from SmA to SmB phase (Fig. 7). However, this transition is accompanied by clear changes of high-angle signal, reflecting molecular ordering within the smectic layer – broad diffused peak characteristic for short-range correlations in SmA becomes much narrower in SmB phase showing increase of in-plane correlation length (Fig. 8). Width of the high-angle signal observed at 100 °C suggest that the mesophase is hexatic smectic B phase rather than a crystal smectic B. In crystalline phase the basic periodicity of the structure is doubled, as evidenced by subharmonic of the main small angle signal.

The tentative scenario of phase transition (during a cooling scan: $I > \text{SmA} > \text{SmB} > \text{Cr}$) was fully confirmed and supported by DSC, POM and XRD.

3.5.3. UV-vis(T) study

UV-vis spectra in different temperatures were measured for thin film on the quartz (film cast from dichloroethane) by using a

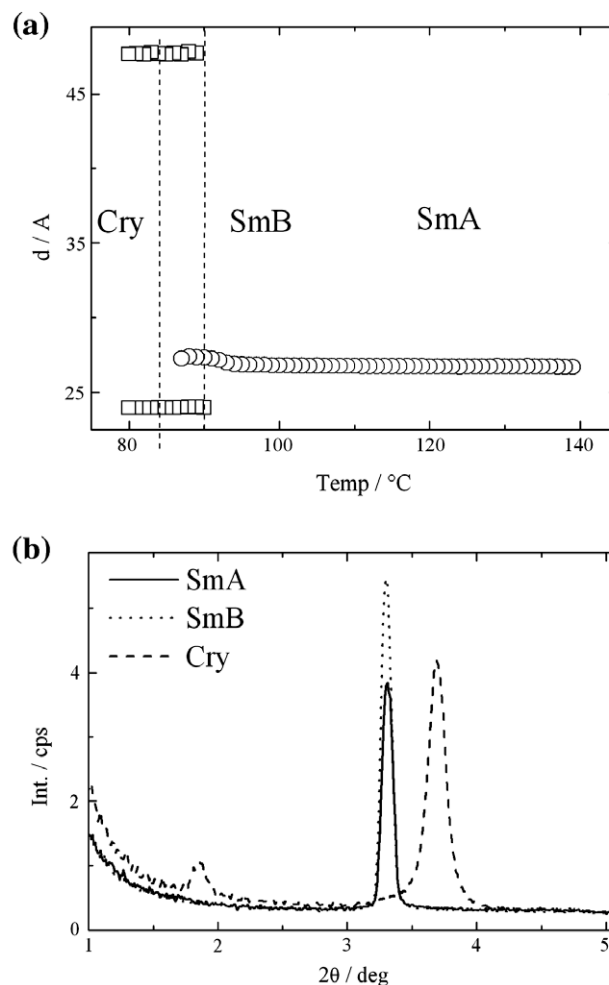


Fig. 7. (a) Temperature dependence of layer spacing for AZ on cooling, (b) small angle X-ray diffraction patterns at $T = 135$ °C (SmA), 100 °C (SmB) and 80 °C (Cry).

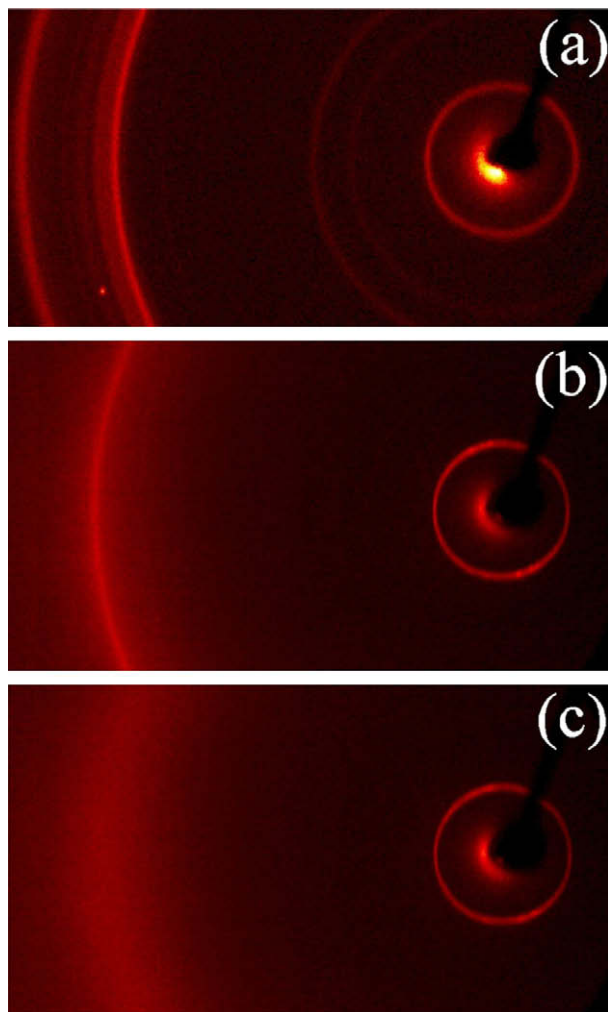


Fig. 8. 2-D wide angle X-ray diffraction patterns at (a) 80 °C, Cry; (b) 100 °C, SmB and (c) 135 °C, SmA.

temperature-controlled optical cell. Fig. 9 shows the UV–vis spectra of the AZ in a temperature range from room temperature to clearing point in the heating process.

UV–vis absorption bands in the azomethine thin film spectrum at ambient temperature were about 40 nm blue shifted in comparison with the one detected in THF solution. This seems to indicate that the conformation of the molecule in solution and in film is different. Moreover, probably this is the case when the transition dipole moments of the molecules are parallel (\parallel) and leading to the formation of so-called H-aggregates, characterized by strongly hypsochromic (blue) shifted UV–vis spectra [25].

In UV–vis spectra of the AZ blue shift of the second absorption band along with increase the temperature was observed (Table 3).

The second absorption band around 311 nm at 25 °C was about 10 nm hypsochromically shifted along with increase the temperature to 105 °C. The absorption band corresponding to the azomethine bond was broader but well defined and was clearly observed to temperature of isotropisation of the AZ appeared at 195 °C. Along with increase the temperature from 25 to 159 °C the second absorption band was 15 nm blue shift along with decreased the absorption intensity (hypochromic effect). The first and third absorption bands were not well defined and exhibited very low intensity (Fig. 9). To find the positions of this band the second derivatives method has been used (i.e., minimum of the second derivative of absorption corresponds to the absorption maximum).

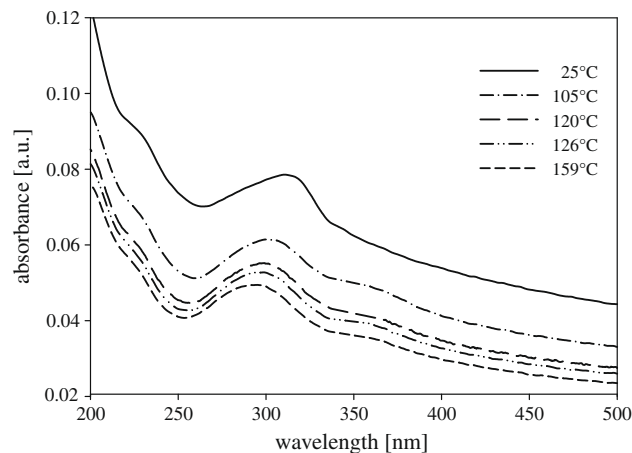


Fig. 9. Temperature dependence of UV–vis spectra of the AZ at the following temperatures: 25, 105, 120, 126, 159 °C.

Table 3
UV–vis absorption characteristic of the AZ.

UV–vis						
Temp. (°C)	λ_1^* (nm)	A_1 (a.u.)	λ_2 (nm)	A_2 (a.u.)	λ_3^* (nm)	A_3 (a.u.)
25	230	0.089	311	0.079	–	–
105	231	0.066	301	0.061	368	0.048
120	231	0.058	298	0.055	365	0.041
126	231	0.055	295	0.053	360	0.039
159	231	0.053	295	0.049	360	0.035

* Position of bands obtained by the second derivative method.

The changes of the absorption spectra along with increase the temperature from 25 to 159 °C can be explained by the geometric isomers (*E* and *Z*) as shown in Fig. 10 and by the aggregation of the AZ at this temperature range to induce tautomerism in the ground state as proposed by Ogawa et al. [26,27]. In the case of the imine structure two isomers are possible (*E* and *Z*), even though the *Z* (*trans*) structure is always supposed to be thermodynamically more stable. Similar behavior was found for the salicylideneanilines and polyazomethines [8,28]. The changes of the absorption properties of the imine along with change the temperature confirmed the conformational changes in the conjugating backbone structure of the compound.

3.5.4. Thermoluminescence study

An example of a typical thermoluminescent glow-curve is illustrated in Fig. 11. The glow-curve consists of a weak single peak located at about 385 K. Its shape was fitted with a first order kinetic-

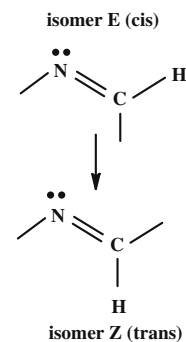


Fig. 10. Schematic structure of the two possible geometric isomers of imine bond.

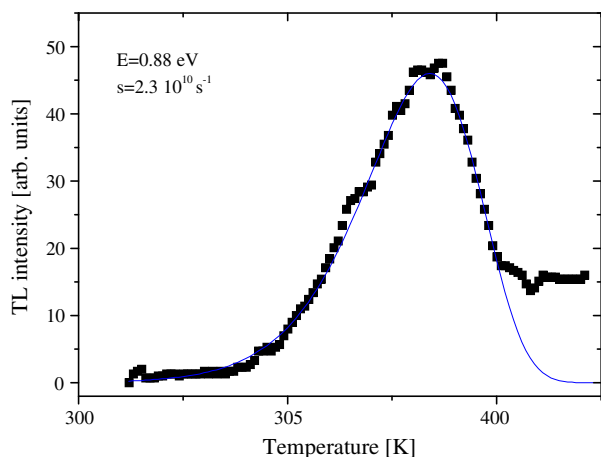


Fig. 11. Thermoluminescent glow-curve of the polymer sample. Symbols – measured data points, solid line – fit with a first order kinetic function. Values of kinetic parameters (activation energy and frequency factor) are shown in the graph.

ics function, using the GlowFit software [29]. It is possible that at lower temperatures also other peaks are present, but as irradiation was performed at room temperature, their life time would be too short to observe them. The measurements were realized using a green filter. When a blue filter was attempted, no TL was observed. This indicates that TL emission occurs at about 500–600 nm wavelengths.

As showed our UV-vis(T) and thermoluminescent experiments the imines can be used potentially as thermo-detectors.

4. Conclusion

The first example of poly(1,4-butanediol)bis(4-aminobenzoate)-based liquid crystalline imine was synthesized and investigated for their phase behavior and optoelectronic properties. The AZ was found to exhibit an enantiotropic smectic A and B phases. The present investigation may be useful for the better understanding of the relation between chemical structure and optoelectronic

and thermal properties of such compounds with imines bonds. For the practical point of view this compound could be applied in organic light-emitting devices, which operating temperature could be higher than room temperature. Additionally, obtained azomethine could be used in mixture with other LCs for LC displays or could be applied as thermo-detectors.

References

- [1] A. Yoshizawa, *J. Mater. Chem.* 18 (2008) 2877.
- [2] F. Vera, J.L. Serrano, T. Sierra, *Chem. Soc. Rev.* 38 (2009) 781.
- [3] T. Kato, N. Mizoshita, K. Kishimoto, *Angew. Chem. Int. Ed.* 45 (2006) 38.
- [4] C. Tschierske, *J. Mater. Chem.* 8 (1998) 1485.
- [5] J.W. Goodby, G.H. Mehl, I.M. Saez, R.P. Tullfin, G. Mackenzie, R. Auzely-Velty, T. Benvegnu, D. Plusquellec, *Chem. Commun.* (1998) 2057.
- [6] B. Donnio, S. Buathong, I. Bury, D. Guillon, *Chem. Soc. Rev.* 36 (2007) 1495.
- [7] C.T. Imrie, P.A. Henderson, *Chem. Soc. Rev.* 36 (2007) 2096.
- [8] A. Iwan, D. Sek, *Prog. Polym. Sci.* 33 (2008) 289.
- [9] D. Ribera, A. Mantecon, A. Serra, *Macromol. Chem. Phys.* 202 (2001) 1658.
- [10] D. Ribera, A. Mantecon, A. Serra, *J. Polym. Sci. A Polym. Chem.* 40 (2002) 4344.
- [11] P.A. Henderson, C.T. Imrie, *Macromolecules* 38 (2005) 3307.
- [12] K. Kishikawa, N. Muramatsu, S. Kohmoto, K. Yamaguchi, M. Yamamoto, *Chem. Mater.* 15 (2003) 3443.
- [13] Y. Naito, R. Ishige, M. Itoh, M. Tokita, J. Watanabe, *Chem. Lett.* 37 (2008) 880.
- [14] S. Sudhakar, T. Narasimhaswamy, K.S.V. Srinivasan, *Liquid Crystals* 27 (2000) 1525.
- [15] V. Cozan, M. Gaspar, E. Butuc, A. Stoleriu, *Eur. Polym. J.* 37 (2001) 1.
- [16] K.S.V. Srinivasan, T. Padmavathy, *Macromol. Symp.* 199 (2003) 277.
- [17] A. Iwan, H. Janeczke, P. Rannou, *Spectrochim. Acta A Mol. Biomol. Spectrosc.* 72 (2009) 72.
- [18] A. Iwan, H. Janeczke, B. Jarzabek, P. Rannou, *Liquid Crystals* 2 (2009) 38 (Materials: special issue).
- [19] E.C. Buruiana, M. Olaru, B.C. Simionescu, *Eur. Polym. J.* 38 (2002) 1079.
- [20] T. Izumi, Y. Naitou, Y. Shimbo, Y. Takamishi, H. Takezoe, J. Watanabe, *J. Phys. Chem. B* 110 (2006) 23911.
- [21] M. Sepelj, A. Lesac, U. Baumeister, H. Loc Nguyen, D.W. Bruce, S. Diele, *J. Mater. Chem.* 17 (2007) 1154.
- [22] R. Bloch, *Chem. Rev.* 98 (1998) 1407.
- [23] D. Demus, L. Richter, *Textures of Liquid Crystals*, first ed., Verlag Chemie, Leipzig, 1978.
- [24] G.W. Gray, J.W. Gooby, *Smectic Liquid Crystals – Textures and Structures*, Leonard Hill, Glasgow & London, 1984.
- [25] J. Gierschner, J. Cornil, H.-J. Egelhaaf, *Adv. Mater.* 19 (2007) 1.
- [26] K. Ogawa, J. Harada, T. Fujiwara, S. Yoshida, *J. Phys. Chem. A* 105 (2001) 3425.
- [27] A. Ohshima, A. Momotake, T. Arai, *J. Photochem. Photobiol. A Chem.* 162 (2004) 473.
- [28] D. Tsang, M. Bourgeaux, W.G. Skene, *J. Photochem. Photobiol. A Chem.* 192 (2007) 122.
- [29] M. Puchalska, P. Bilski, *Radiat. Meas.* 41 (2006) 659.